2020

Bench-Scale Investigation of Remote Detection of Clay Pockets in Granular Soils

Nick W. Hudyma
Boise State University

Brian Kopp
University of North Florida

Joshua Oglesby
University of North Florida

Sukris Vong
University of North Florida

Bench-Scale Investigation of Remote Detection of Clay Pockets in Granular Soils

Nick W. Hudyma, Ph.D. P.E., M. ASCE
Department of Civil Engineering
Boise State University
Boise, ID
nickhudyma@boisestate.edu

Brian Kopp, Ph.D.
School of Engineering
Electrical Engineering Program
University of North Florida
Jacksonville, FL
brian.kopp@unf.edu

Joshua Oglesby
School of Engineering
Civil Engineering Program
University of North Florida
Jacksonville, FL
n00944734@unf.edu

Sukris Vong
School of Engineering
Electrical Engineering Program
University of North Florida
Jacksonville, FL
n01050608@unf.edu

Abstract

The detection of deleterious materials in compacted soil fills is an important part of earthwork construction. These materials are often identified *a-priori* using laboratory techniques such as the visual assessment of sieve analyses. However, it is possible that deleterious materials, such as clay pockets, can be larger than particles characterized in laboratory tests. Bench scale imaging using simulated unmanned aerial vehicle flights were conducted to determine if clay pockets, 15.24 cm by 15.24 cm by 5 cm thick, could be detected in granular soils. The imaging techniques employed were digital imaging, thermal imaging, and electromagnetic imaging. All imaging techniques could be used to identify clay pockets at the surface, but only electromagnetic imaging could detect clay pockets beneath the surface. The clay pockets were easily identifiable at depths of 2.5 cm and 15.2 cm in fine sand. When buried in pea gravel, the clay pockets were identifiable only at a depth of 2.5 cm. The clay pockets could not be identified when buried in gravel sized particles.

Introduction

The presence of deleterious materials has a negative effect on the quality or performance of engineered materials such as concrete, asphalt pavements, and compacted soils. For compacted soils the deleterious materials may come from two sources, it may be inherent to the parent material or come from contamination. The contamination may be naturally or artificially generated (Richardson, 2009).

Deleterious materials in soils can be grouped into the following categories: oversized materials, organic materials, unsound particles, debris, clay material, frozen material, saturated material, and other foreign materials (OFM). Within each of these categories, there are a number of pre-identified materials, based on geographic location, which are considered deleterious. For example, in the unsound particle category the following materials have been listed by various state agencies: shale, mica, soft and flaky particles, soft rock, coal and lignite, argillaceous rock, laminated particles, limonite, lightly cemented rock or particles, rock with weak crystal structure, weathered rock, shells, and ochre. The list contains both specific examples (mica) and general examples (laminated particles).

Deleterious materials can be identified by a variety of laboratory aggregate-based tests. A summary of these aggregate-based tests is provided by Richardson (2009). The most common laboratory test to determine the presence of deleterious material in soils is a sieve analysis with a visual inspection of particles retained on each sieve. Aggregate based tests are not applicable to deleterious materials which are larger than the typical soil size used in construction.

This study is focused on the remote detection of deleterious clay materials within granular soils. Deleterious clay materials are often described as mudballs, clay pockets, clay lumps, or clay coated aggregates. The underlying assumption of the study is that the clay pockets are much larger than the largest grain size of the soil. Such deleterious materials could be identified in the field through manual inspection and probing but such activities place construction personnel in dangerous situations. Using remote sensing techniques with mapping capabilities and potentially machine learning algorithms can provide both a safe working environment and potentially a more accurate methodology for detecting clay pockets in compacted soils.

Bench Scale Apparatus

The bench scale apparatus consisted of six bins, as shown in Figure 1. The bins were made of 12.7 mm thick acrylic plates which were epoxied together. The inside dimensions of the bins were 29.2 cm tall by 30.5 cm wide and 58.4 cm long. They were placed side by side and supported by 89 mm x 89 mm lumber stringers running the combined width of the bins, 89 mm x 89 mm lumber beams orientated perpendicular beneath the stringers, and cinder blocks supporting the beams. It was necessary to have an air space beneath the bins so that electromagnetic absorbing anechoic foam panels could be placed beneath the bins. The construction of the bins, support system, and incorporation of the foam panels minimized stray electromagnetic wave reflections during imaging.

The six bins were filled with three different sizes of washed oven-dried granular soil. The large aggregate was crushed limestone which passed the 37.5 mm sieve and was retained on the 12.5 mm sieve. The pea gravel was crushed limestone which passed the 12.5 mm sieve and was retained on the 4.75 mm (#4) sieve. The sand, which was predominantly silica sand, passed the 840 μm (#20) sieve and was retained on the 740 μm (#200) sieve. All materials were placed loosely in the bins.

The clay pockets were 15.24 cm by 15.24 cm by 5 cm thick cuboids of pottery clay. The moisture content of the clay was approximately 22%.

Two tripods were placed at the ends of the lumber stringers. The tripods were used to support a rail system on which two small nylon wheeled trolleys with mounting fixtures were able to traverse the combined width of the bins. The rail system was constructed of aluminum angle stock. A metal measuring tape was attached to the outside of the rail system which was used to monitor the location of the trolleys during the imaging runs. The inner width of the rail system was 16.19 cm. The trolleys measured 17.78 cm in length from the outer edge of the axels and were the width of the rail system. The imaging tools were mounted to either one or both trolleys. Figure 2 shows the rail system and one of the trolleys.

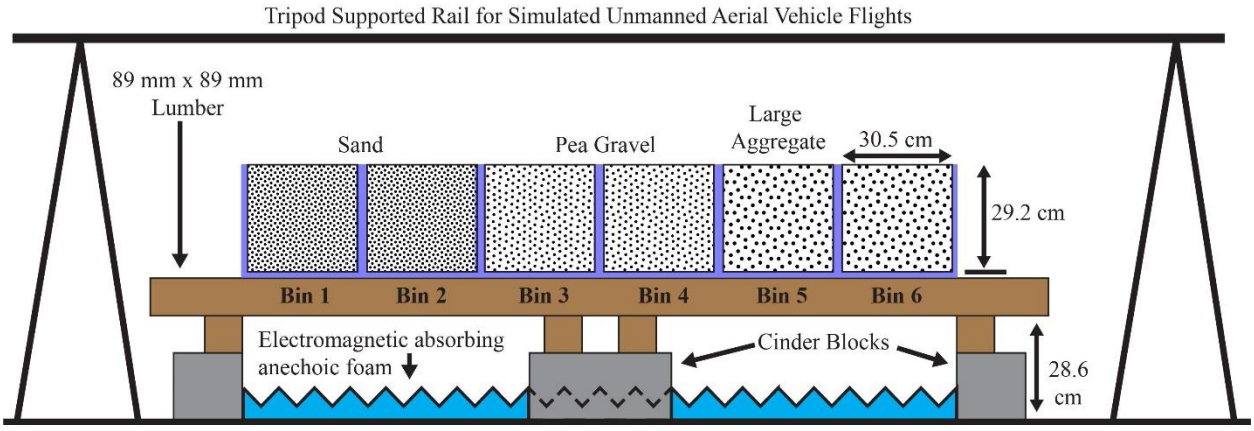

Figure 1. Bench scale setup for simulated unmanned aerial vehicle flights over bins.

Figure 2. Rail system and trolley for mounting imaging equipment.

Imaging Techniques

Three different imaging techniques were used to identify clay pockets within the three different sizes of granular soils. The imaging techniques were digital imaging, thermal imaging, and electromagnetic imaging. Each of the techniques are described below.

Digital Imaging. A Canon EOS DSLR 200D with an 18-135 mm variable focal length lens was used for the digital imaging. Digital imaging consisted of collecting single overlapping images of the surface of the granular soils within the bins and then developing a single orthomosaic image. The DSLR camera was attached to a trolley using a camera mount and incrementally moved along the rail system to obtain the overlapping images. Multiple camera passes with the rail system near the left and right edges of the bins were required to develop the orthomosaic images.

Thermal Imaging. A handheld FLIR E60 thermal camera was attached to a trolley using a camera mount and moved incrementally along the rail system to obtain thermal images. The camera has an image resolution of 320 × 240 pixels. Thermal images were used to determine if the clay pockets could be identified, both at the surface and at depth, based on thermal signatures.

Electromagnetic Imaging. An electromagnetic (EM) wave transmitter and receiver were attached to the trolleys and aimed downward at the aggregates using matching incident and reflected angles. The EM wave frequency chosen for this study was 10.4 GHz based on the dimensions and materials used in the bench scale apparatus. This frequency is an amateur frequency which minimized radio transmitter licensing issues. There is a commercial frequency band next to this amateur spectrum, at 11 GHz, that could be leveraged for future large-scale testing and field implementations. The microwave transmitter was designed using a Gunn oscillator and isolator attached to a pyramidal feedhorn antenna. The isolator was necessary to reduce intermodulation in the oscillator from backscatter energy at the nearby target material. The wavelength of the 10.4 GHz EM wave in air is approximately 2.9 cm.

The arrangement of the EM wave transmitter and receiver is shown in Figure 3. For both the transmitter and receiver feedhorns (Fig. 3B), the half power beam width of the linear electric field is 30 degrees, producing a gain of 17 dB in each feedhorn. The feedhorns are rectangular-base pyramidal horns with the electric field perpendicular to the long axis of the base, meaning the EM wave beam is wider in the electric field direction than in the perpendicular magnetic field direction. To ensure the majority of the EM wave would illuminate only aggregate in the bins, the rail-mounted height of the feedhorns was limited.

The pyramidal horns were fixed at 32.7 cm above the soil surface. The horizontal separation between the transmitter and receiver was fixed during each test but was varied depending on the required imaging. A laser pointer was used to ensure the two feedhorns were pointing at the same spot on the soil surface with matching incident and reflection angles. Once configured, the horizontal distance was recorded so that the angles could be calculated. The test profiles used angles ranging from 22.9° to 33.3°. Readings were taken every centimeter across the bins. The active EM

reflecting off a material boundary and the nature of the reflected energy (amplitude, time delay, etc.) conveys information about the sub-surface material beyond the boundary. This technique is referred to as EM backscatter (Daniels et al., 1988).

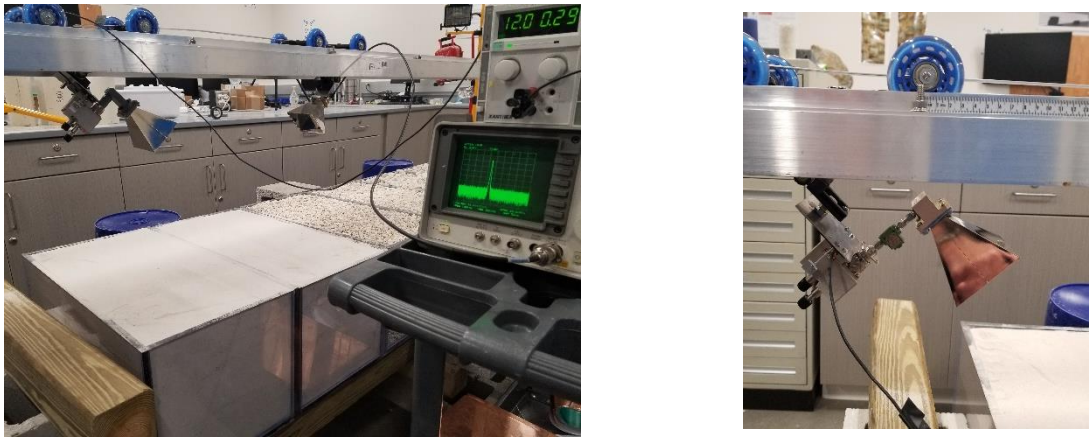

A. EM imaging over sand. **B. Closeup of tansmitter feedhorn.**

Figure 3. Electromagnetic imaging system.

The EM imaging system was calibrated using copper sheets placed on top of the bins. During calibration, the transmitted EM wave reflected off the copper sheets and into the receiver. The height was set at 27.0 cm and the horizontal distance to the reflection point was 11.4 cm. This created an incident angle of 22.9° and an EM wave path length of 58.6 cm. The received EM wave power during calibration was recorded as -2 dBm (dB referenced to one milli-Watt). The expected free-space-loss attenuation at 58.6 cm is 48 dB. Using the gains of the two feedhorns, the power from the oscillator was back calculated to be 12 dBm which matches closely with the Gunn oscillator rated output.

Imaging Results and Discussion

Imaging was conducted in three stages. The first imaging stage, termed baseline imaging, was conducted on granular soil without clay pockets. For the second imaging stage, clay pockets were set into the granular soil but exposed on the surface. The third imaging stage was conducted with the clay pockets buried at predetermined depths within the granular soil. Results of the imaging are presented below.

Granular Soil Imaging. Baseline imaging was conducted to assess whether the different aggregate sizes could be detected using digital and EM imaging. Results from the two imaging techniques are presented in Figure 4. As expected, it was possible to visually distinguish the three aggregate sizes with digital imaging (Figure 4A). Individual grains could be identified in the pea gravel and the large aggregate, but it was not possible to identify individual grains within the sand.

A. Orthomosaic image.

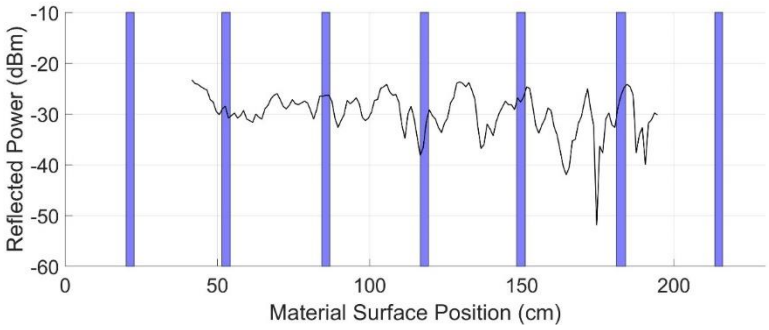

B. EM imaging.

Figure 4. Results from granular soil imaging.

The EM imaging (Fig. 4B) is presented as a reflected power value with units of decibels relative to one milliwatt (dBm). The colored lines represent the edges of the acrylic bins. The increased roughness of the aggregate surface presents as an increase in variation of the magnitude of the reflected EM wave (Fig. 4B). Although rearranging the more coarse material changed the locations of maximum and minimum received power levels, the variability and the slight decrease in average received power appeared similar. Rearranging the fine sand had no apparent effect on the reflected EM wave power that was received.

Imaging with Clay Pockets Exposed on the Surface. Digital imaging, thermal imaging and EM imaging were conducted to assess if clay pockets could be detected at the aggregate surface. The clay pockets were 15.24 cm by 15.24 cm by 5 cm thick and centered on the left edge of bins two, four, and six. Imaging results are presented in Figure 5. As expected, using digital imaging (Fig. 5A), it was possible to visually distinguish the exposed clay pockets within the granular soils. The clay pockets have a distinct shape and brown coloring compared to the whitish colored soils.

Thermal imaging was also successful in distinguishing the surficial clay pockets (Fig. 5B). The granular soils were in an oven-dried condition and the clay pockets were moist with a moisture content of approximately 22%. The thermograms clearly show the clay pockets with a cooler temperature than the surrounding dry soil. The resolution of the thermal camera was not high enough to visually distinguish individual particles in the sand and pea gravel.

A. Orthomosaic image.

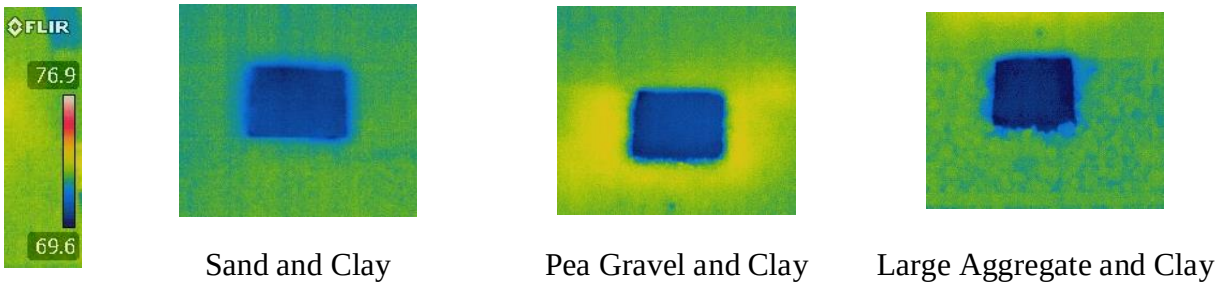

B. Thermal images.

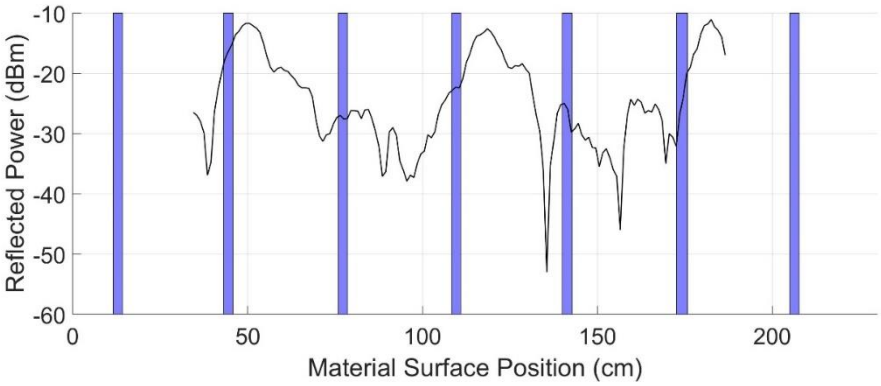

C. EM imaging.

Figure 5. Results from imaging with clay pockets exposed at the soil surface.

The EM imaging shows distinct peaks in the reflected power for the surficial clay pockets for all soil sizes. The sand had a reflected power of approximately -30 dBm. The pea-gravel had an average reflected power of approximately -26 dBm. The large aggregate had an average reflected power of approximately -35 dBm. Regardless of the soil size, the reflected power from the clay pocket peaked at approximately -11 dBm.

Imaging with Clay Pockets Beneath the Surface. Thermal and EM imaging were conducted to assess if the clay pockets could be detected below the surface of the granular soils. Surprisingly the thermal imaging was not successful in detecting the clay pockets when buried 2.5 cm beneath the surface of the soils. Figure 6 shows the results of the EM imaging with the clay pockets centered on the left edge of bins two, four, and six at depths of 2.5 cm and 15.2 cm.

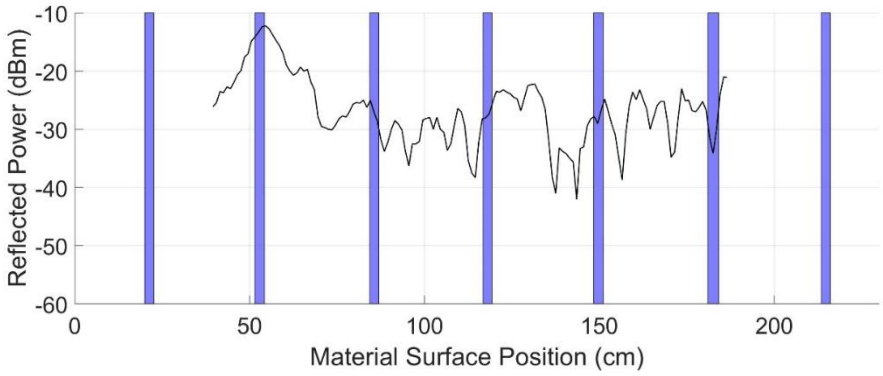

A. EM imaging with clay pocket at 2.5 cm depth.

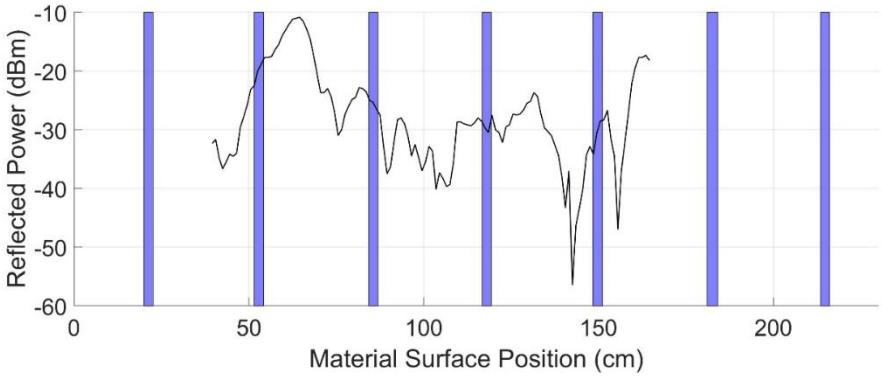

B. EM imaging with clay pocket at 15.2 cm depth.

Figure 6. Results from imaging with clay pockets beneath the surface.

When buried at a depth of 2.5 cm, the clay pocket was identifiable in the sand. The reflected power was similar to the reflected power obtained from the clay pocket at the surface. There was a reduction in reflected power from buried clay pocket in the pea gravel, but the reflected power was -22 dBm whereas the reflected power received when the clay pocket was at the surface was -11 dBm. The results were inconclusive for the large aggregate.

When buried at a depth of 15.2 cm, the clay pocket was still identifiable in the sand. The results were inconclusive for both the pea gravel and large aggregate. As the clay was buried at greater depths the distance traveled by the trolley was reduced because the incident angle of the EM wave meant the clay was imaged from a progressively earlier trolley position. This explains the shortened graphs.

Summary

The issues with deleterious materials in compacted soils is well understood by both geotechnical engineers and contractors. There are numerous laboratory-based tests which are used to identify deleterious materials however it would be advantageous to have a remotely operated field-based system to detect deleterious materials during construction operations. In this study, a bench scale apparatus was developed and deleterious clay pockets were placed in bins containing three different sizes of oven-dried granular soil. Simulated drone flights were conducted using digital imaging, thermal imaging, and electromagnetic imaging to detect clay pockets both on the surface and below the surface.

Orthomosaic images were developed from overlapping digital images. Using the orthomosaic images, it was possible to visually distinguish the three sizes of granular soils and the clay pockets exposed on the surface of the granular soils. Using thermal imaging, it was possible to distinguish the moist clay pockets from the oven-dried granular soils. However, when the clay pockets were buried 2.5 cm below the soil surface thermal imaging could not detect the clay pockets.

An electromagnetic (EM) imaging system using transmitter and receiver pyramidal horns was also used for imaging. The system transmitted an EM wave with a frequency of 10.5 GHz and an air wavelength of 2.9 cm. Reflected power was recorded as the EM imaging system was moved in centimeter increments across the soil. It was possible to distinguish the three different soil particle sizes using the EM imaging; the larger the particle size the more undulating the reflected power signal. It was possible to detect clay pockets at the surface of the aggregate bins because the reflected power was lower from the clay pockets than the soils. Clay pockets buried at a depth of 2.5 cm could be detected in the sand in the sand and pea gravel. Clay pockets could be detected at a depth of 15.2 cm in the sand but not in the pea gravel. The success of the simulated airborne EM imaging to detect clay pockets on the surface and at depth is promising and additional studies are being conducted to optimize the EM system to work for moist compacted soils so that real world scenarios can be investigated.

References

Daniels, D.J., Gunton, D.J., and Scott, H.F. (1988). "Introduction to Subsurface Radar". *IEEE Proceedings F – Communications, Radar and Signal Processing*, 135(4), 278-320, 10.1049/ip-f-1.1988.0038.

Richardson, D.N. (2009). "Quick test for percent of deleterious material". Final Report RI07-052 Prepared for the Missouri Department of Transportation. <https://library.modot.mo.gov/rdt/reports/ri07052/or10005.pdf>